POLYCAPROLACTONE BASED NANOFIBER SCAFFOLDS CAN MIMIC COLLAGEN FIBRIL DIAMETER DISTRIBUTION OF HEALTHY AND INJURED SHEEP ANTERIOR CRUCIATE LIGAMENT

Smail Smatov, MSc of Chemical and Materials Engineering

School of Engineering and Digital Sciences

Department of Chemical and Materials Engineering

Nazarbayev University

53 Kabanbay Batyr Avenue,

Nur-Sultan, Kazakhstan, 010000

Lead Supervisor: Cevat Erisken, Ph.D.

Department of Chemical and Materials Engineering

2021

Declaration

I hereby, declare that this manuscript, entitled “Polycaprolactone based nanofiber scaffolds can mimic collagen fibril diameter distribution of healthy and injured sheep anterior cruciate ligament” is the result of my own work except for quotations and citations which have been duly acknowledged.

I also declare that, to the best of my knowledge and belief, it has not been previously or concurrently submitted, in whole or in part, for any other degree or diploma at Nazarbayev University or any other national or international institution.

Name: Smail Smatov

Date: 10.12.2021

Acknowledgments

I am deeply grateful to all people for their valuable effort and contribution to this research work. I would like to express my sincere gratitude to my thesis supervisor Dr. Cevat Erisken, for patience, assistance, guidance and recommendations at every stage of the research project. He inspired me to study novel fields in science including tissue engineering and biomechanics.

I am also grateful to my laboratory colleagues Fariza Mukasheva, Bakhytbol Khumyrzakh, Sanazar Kadyr for their encouragement and help with the experiments. Their supporting words and feedback have always been a great source of motivation.

In addition, I wish to acknowledge the help provided by Nurgul Daniyeva and Laura Khamkhash in conducting TEM and SEM characterizations.

Last but not the least, I must express my endless gratitude to my family. My mother Rezida Smatova, brother Ansar and my sisters Kamilla and Yasmin. Mom, thank you for supporting me throughout my life! My brother and two sisters, thank you for your motivation and encouragement. To my family, I have devoted everything, including this.

Table of Contents

List of abbreviations

ANOVA	Analysis of variance
AA	Acetic acid
ACL	Anterior cruciate ligament
ECM	Extracellular matrix
FA	Formic Acid
FATC	Femur-ACL-Tibia complex
MSC	Mesenchymal stem cell
PBS	Phosphate buffer solution
PEUUR2000	Poly (ester urethane urea) elastomer
PGA	Poly(glycolic acid)
PCL	Poly(caprolactone)
PLA	Poly(lactic acid)
PLGA	Poly(lactic-co-glycolic acid)
PLLA	Poly(L-lactic acid)
PUR	Poly(urethane)
SEM	Scanning Electron Microscopy
TEM	Transmission Electron Microscopy

List of Tables

List of Figures

Abstract

A ligament is a soft connective tissue with a hierarchical structure that attaches bone to bone. The Anterior Cruciate Ligament (ACL) tissue connects femur and tibia, and possesses low potential for self-regeneration due to its hypovascularity and hypocellularity. ACL injuries in the knee joint are prevalent among the people actively involved in sports such as basketball, football and skiing. Unfortunately, currently available clinical treatments cannot fully restore the injured tissue as indicated by low success rates in clinical procedures. Tissue engineering strategies can provide alternative approaches with a potential of restoring the injured ligaments by employing biomimetic scaffolds that are similar to native tissue in terms of structure, composition and functions.

Here, it is hypothesized that the electrospun fibers with bimodal and unimodal distributions will mimic the collagen fibril diameter distribution of healthy and injured sheep ACL, respectively. To test this hypothesis, it was aimed to, firstly, create an injured sheep ACL by applying mechanical loading to the healthy ACL tissue until rupture. Secondly, Transmission Electron Microscopy (TEM) characterization was performed on the healthy and injured ACL tissues to determine collagen fibril diameter distributions. Thirdly, Polycaprolactone (PCL) scaffolds were produced via electrospinning method to mimic the bimodal and unimodal distributions of collagen fibrils in the healthy and injured tissues. Finally, mechanical characteristics of ACL and PCL electrospun scaffolds were determined at a crosshead speed of 5 mm/min in tension.

Findings of this study demonstrated that the bimodal distribution of collagen fibril diameter of ACL changes to unimodal upon injury, resulting in a reduction in mean diameter. The fiber diameter distributions of polycaprolactone electrospun scaffolds were shown to mimic the collagen fibril diameter distribution of healthy and damaged ACL. In terms of biomechanical characteristics, native ACL tissue outperformed PCL scaffolds. Aligned bimodal scaffolds exhibited improved mechanical properties as compared to unaligned unimodal PCL scaffolds.

This study is novel because we demonstrated, for the first time, the collagen fibril diameter distribution of healthy and injured ACL tissues harvested from sheep. Additionally, we propose a method for fabrication of scaffolds that mimic the collagen fibril

diameter distribution of healthy and injured ACL. The study's significance relies on the fact that it addresses an important clinical problem related to orthopedics that concerns millions of patients worldwide. The fibrous scaffold design proposed here deviates from the traditional unimodal technique, and it is anticipated to have a substantial impact on ACL regeneration efforts.

Keywords: ACL, PCL, tissue engineering, nanosized fibers, biomimicry, ligament scaffold, polymer fiber-based fibers, electrospinning, mesenchymal stem cells.

1. Introduction

Tissue engineering has a great potential for the restoration and regeneration of damaged soft tissues as well as soft tissue to bone interfaces because it offers a strategy to combine cells, scaffolds and biomolecules to create native-like structures. This thesis project characterizes the native sheep ACL tissues and proposes a method to produce biomimetic scaffold to be later utilized for the regeneration of the soft tissue part of the ACL to bone interface. The enrichment of these scaffolds with biomolecules and their cellularization to generate ligament-like tissues are beyond the scope of this thesis.

1.1 ACL Injuries and Current Restoration Approaches

ACL related injuries represent a significant portion of musculoskeletal related injuries, with around 4 million annual cases worldwide [1]. Annually, there are 77.4 per 100,000 people ACL reconstruction procedures worldwide [2]. This number is increasing annually among the professional sportsmen by 3% [3]. It is reported that the majority of ACL injuries are among football players, skiers and professional athletes [4]. ACL injuries, if left untreated, can lead to secondary complications such as cartilage and meniscus damages, knee laxity, dysfunctionalities of movement and the early stage of post-injured osteoarthritis [1] because ACL has limited self-healing capacity due to hypocellularity and hypovascularity [5]. In this regard, tissue engineering or utilization of synthetic/natural grafts stand as alternative approaches to regenerate/repair the ACL traumas via surgical intervention.

According to Silvers & Mandelbaum, there are three types of ACL injuries [6]:

I. The size of tear is less than 33.3% of the ligament fibers and the fragility of knee is less than 5 mm.
II. The size of tear varies from 33.3% to 66.7% in the ligament fibers and the fragility reaches to 10 mm
III. The size of tear is more than 66.7% of the ligament fibers and the fragility varies from 10-15 mm.

The functionality loss is visible on the second and third grades. The most of injuries involve the sudden changes of direction, movement and landing from a jump with hip flexion and not-full knee extension [6].

Currently available clinical approaches for restoring the torn/ruptured ACL are based on surgical, nonsurgical and rehabilitation procedures. The surgical method includes replacement of the torn/ruptured ACL with grafts extracted from native tendons [7]. This method of ACL treatment comes with some drawbacks such as the immunological response to the transplanted graft (in the case of allograft or xenograft) and inferior mechanical and physiological properties. Another surgical method with the use of synthetic grafts eliminates the possibility of immune response yet lacks some of the important properties of the native grafts including compositional, structural and thus functional similarity [8]. The nonsurgical approach, on the other hand, includes the intensive and controlled management of exercises under the guidance of a physiotherapist. This method is recommended for people who are not actively involved in sport and cannot be an option for patients with ruptured or massively torn ligaments.

1.2 Ligament-to-bone interface structure

The native ligament-bone connection is constituted of gradients of different tissues, such as ligament, bone and fibrocartilage, involving multiple cell phenotypes such as osteoblasts, fibrochondrocytes and fibroblasts in corresponding zones [9, 10]. The fibrocartilage tissue is further divided into non-calcified and calcified regions. Current ligament restoration of grafts with mechanical fixation has been shown to fail to reinstate this hierarchical ligament-to-bone transition after surgery [11, 12]. As a result, novel augmentation matrices are required to promote biological fixation and scarless healing at the ligament-to-bone contact.

1.3 ACL Anatomy, Structure and Composition

The ACL connects femur (thighbone) and the tibia (shinbone) together with posterior cruciate ligament, is located in and stabilizes the knee joint (Fig.1). ACL limits the lower leg from excessive movement and holds the outer condyle of the tibia. The ACL can sustain the mechanical loads due to its alignment of collagen fibers. Their alignment is arranged transversely, longitudinally and horizontally that is responsible for the proper management of forces exerted during the motion [1].

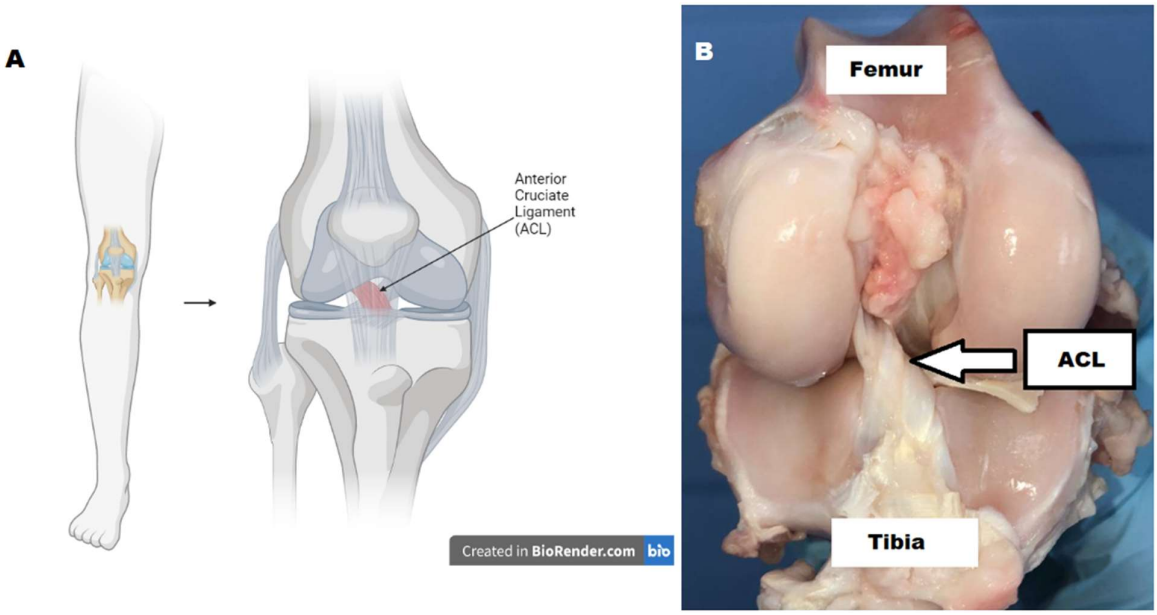

Figure 1. A – Anatomical structure of human ACL (Drawn at and retrieved from: BioRender.com), B – anatomical structure of sheep ACL

ACL tissue consists of water (approximately two-third by mass) and solid materials. Biochemical composition of solid structure is 75% (by weight) collagen of type I (85%) and the rest contains collagen types III, VI, V, XI and XIV. The remaining 25% is balanced between proteoglycans (<1%), elastin and glycoproteins [13]. Collagen fibrils of ACL have diameter ranging from 25 to 250 nm. There are two types of fibrils: first type is secreted by fibroblasts and has diameters around 35, 50 and 75 nm [14]. The first type accounts for approximately 50% of the fibrils [14]. The second type has a peak diameter of about 45 nm and is secreted by fibro-chondroblasts [14]. It accounts for about 44% of the total fibrils. The other 6% are divided by matrix components and cells [14].

The microstructure of ACL is shown in Fig.2. The ligament is comprised of grouped fascicles with diameters ranging from 50 to 300 μm [15]. The next level is fibrils with diameters from 50 to 500 nm [16]. The aligned collagen fibrils are oriented along the axis of ACL, which contributes to tissue's mechanical resilience and strength.

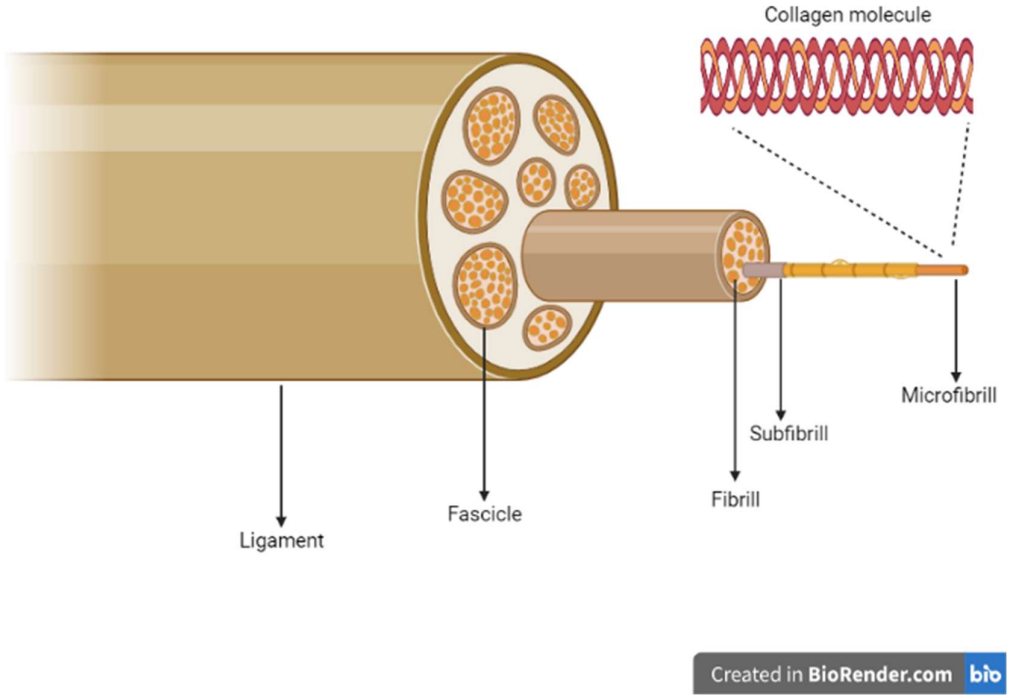

Figure 2. The hierarchical microstructure of ligament. Drawn at and retrieved from: BioRender.com

1.4 Biomechanical characteristics of ACL

The biomechanical behavior of ACL tissue during the tensile loading was reported to start with a toe region followed by linear and yield regions, and end with failure as shown in Fig.3 [17].

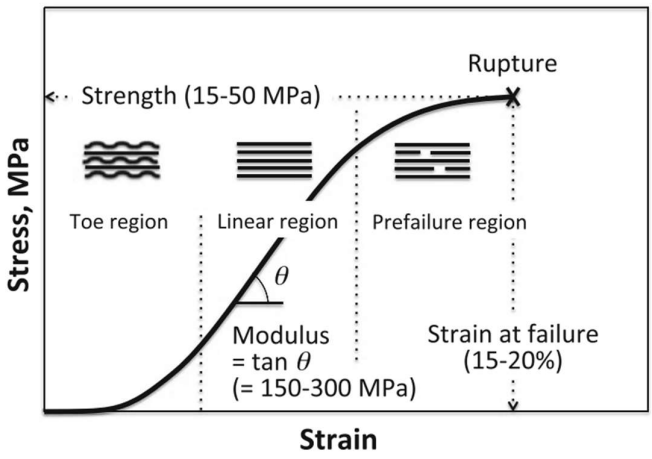

Figure 3. ACL Stress-strain relationship and the explanation of mechanical properties. Retrieved from: [17]

The toe region is where the wavy fibrils are aligned in the direction of tension. In the linear region, force rises linearly with elongation, exhibiting an elastic deformation. The beginning of permanent deformation occurs in the prefailure region. In this area, decrease of the stress is explained by the disarrangement or partial rupture of collagen fibrils, ultimately leading to the rupture of ligament.

Strain-energy density is the parameter which shows the energy stored during deformation [18]. The strain-energy density is equal to the area under the stress-strain curve that includes toe and linear regions which can reveal the stored energy of native ACL tissue upon elastic deformation. Poisson's ratio is defined as the change of material's dimension as the material deforms [19]. The Poisson's ratio for ACL tissue for sheep was estimated as 0.4 indicating that the ligament tissue is ductile [20].

The mechanical characteristics of ACL tissue for several species are presented below (Table 1).

Species	Age/Weight	Strain rate (mm/min)	Stiffness (N/mm)	Maximum load (N)	Source
Rat	279g	5	37.5 ± 11.5	47.8 ± 9.2	[21]
Sheep	9 months	5	144.97 ± 35.34	548.78 ± 41.44	[22]
Sheep	4 months	6	136.3 ± 28.5	759.2 ± 114.1	[23]
Sheep	NR	60	44.5 ± 12.5	1531.3 ± 180.3	[24]
Porcine	Not reported	5	43.5 ± 7.1	1055.5 ± 151.2	[25]
Human	22–35 years	20	242 ± 28	2160 ± 57	[26]
Bovine	3-7 years	60	577.3 ± 483.1	4372 ± 1485	[27]
Bovine	12 months	500	204.1 ± 89.5	3317 ± 819	[28]
Bovine	Mature	60	NR	4541 ± 1417	[29]

Table 1. Mechanical properties of ACL for different species. Retrieved from: [30]

Butler (1992) characterized the mechanical properties of ACL at a strain rate of 1 s^{-1} (Table 2) [31].

Property	Unit	Anteromedial bundle	Anterolateral bundle	Posterior bundle
Modulus	MPa	283.1 ± 114.1	285.9 ± 140.6	154.9 ± 119.5
Strength	MPa	45.7 ± 19.5	30.6 ± 11.0	15.4 ± 9.5
Strain at failure	%	19.1 ± 2.8	16.1 ± 3.9	15.2 ± 5.2

Table 2. Human ACL material properties with different bundles. Retrieved from: [31]

1.5 Collagen fibril diameter of ACL tissues

The diameter of collagen fibrils was previously reported to alter from bimodal to unimodal distribution with decreased average fibril diameter (Table 3).

Species	Peak for healthy tissue (nm)		Range Healthy (nm)	Peak value for injured tissue (nm)	Range Injured (nm)	Reference
	Smaller	Larger				
Mouse AT	~50	~170	10 – 320	NR	NR	[32]
Mouse FT	~60	~270	40 – 400	NR	NR	[33]
Mouse PT	~50	~145	15 – 215	~45	15 – 125	[34]
Rat PT	~50	~210	20 – 380	~50 & 170	20 – 380	[35]
Rabbit ACL	~20	~250	10 – 320	NR	NR	[36]
Rabbit MCL	~40	~190	20 – 270	NR	NR	[26]
Sheep ACL	~60	~200	20 – 300	NR	NR	[37]
Human ACL	~50	~150	20 – 200	NR	NR	[38]
Human ACL	~75	NR	20 – 185	71	20 – 290	[39]
Human ACL	~35		10 – 125	NR	NR	[40]
Bovine ACL	~60	~120	40 – 250	NR	NR	[41]
NR: Not reported, PT: Patellar Tendon, MCL: Medial Collateral Ligament, FT: Flexor Tendon, AT: Achilles Tendon						

Table 3. Values of fibrill diameter of different adult species. Retrieved from: [30]

1.6 Material selection and scaffold fabrication

The choice of biomaterial for scaffold and its production method have significant impact on the functional properties of the scaffold. At least, the following parameters should be considered during selection of the material:

I. Biocompatibility: This implies that the material should have minimal adverse effects when comes into contact with the host environment [42].
II. Biodegradability: Refers to the controlled degradation of the biomaterial over time as cells synthesize new extracellular matrix [42].
III. Porosity: This determines the void content of the scaffold through which cells can infiltrate [43].
IV. Morphology: Materials should allow for the generation of structures and surface properties that mimic the native tissues [44].
V. Mechanical properties: These affect cellular differentiation, proliferation and the production of ECM [45].

Previous studies investigated polymer-based materials for ligament as well as ligament-to-bone interface regeneration including PLGA (poly(lactic-co-glycolic acid)), PCL (poly(caprolactone)), PUR (poly(urethane)), PEUUR2000 (poly(ester urethane urea) (Table 4).

Acronym	Extended name	Sources
PLGA	poly(lactic-co-glycolic acid)	[46] [47] [48] [49]
PCL	poly(caprolactone)	[46] [47] [50] [51][52] [53] [54] [55] [56]
PUR	poly(urethane)	[51]
PEUUR2000	poly(ester urethane urea) elastomer	[50]

Table 4. Polymers used in previous studies for ligament-to-bone interface regeneration.

Structural, biochemical and mechanical properties of the final scaffold rely on the fabrication method and the material of construction. The most frequently used aliphatic polyesters for soft-to-hard tissue interface are presented in Table 5.

Polymer	Tensile strength (MPa)	Young's modulus (MPa)	Ultimate strain (%)	Biodegradation time (months)
PCL	20.7 – 34.4	210 – 340	300 – 500	24 – 36
PLGA	41.4 – 44.2	1400 – 2800	3 – 10	2 – 3
PGA	68.9	>6900	15 – 20	6 – 12
L-PLA	59	1280	7	12-16
PLLA	27.6 – 41.4	2700 – 4140	3.0 - 10.0	>24

Table 5. Mechanical properties and biodegradation time of biopolymers. Retrieved from: [46, 47]

PCL was selected as the material of construction for the scaffolds because of its low cost, ease of electrospinability and suitability in terms of mechanical properties. Additionally, PCL is approved by the Food and Drug Administration to be used as a biomaterial for medical devices.

Amongst available techniques for scaffold fabrication including particle leaching, phase separation, 3D printing and electrospinning, the method of electrospinning possesses the advantages of being a versatile method that allows for the low-cost production of nanostructures with desired and controlled fiber organization [59].

Parameters of the electrospinning method:

I. Solution parameters: viscosity of solution, molecular weight of polymer, solution conductivity, surface tension, dielectric constant boiling temperature of solvents [60].
II. Process parameters: flow rate of the extrusion, the applied voltage, the distance between the collector plate or drum and the needle, the diameter of needle.
III. Environmental parameters: temperature, relative humidity and pressure [61].

2. Materials and methods

Experimental part of this study comprises several steps:

I. Harvesting and characterization of native ACL tissues from sheep.
II. Electrospun scaffold fabrication and characterization via SEM/TEM.
III. Tensile biomechanical characteristics of ACL tissue and PCL scaffolds.

Experimental procedure is demonstrated in Figure 4.

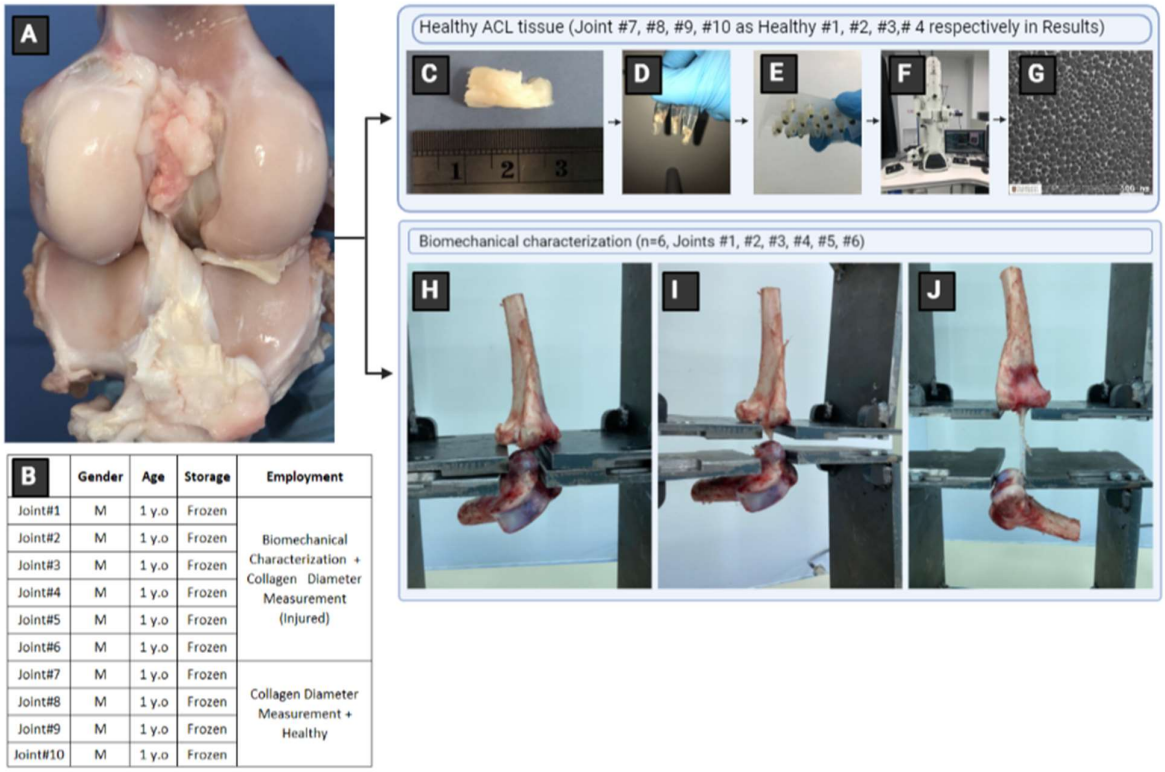

B	Gender	Age	Storage	Employment
Joint#1	M	1 y.o	Frozen	Biomechanical Characterization + Collagen Diameter Measurement (Injured)
Joint#2	M	1 y.o	Frozen	
Joint#3	M	1 y.o	Frozen	
Joint#4	M	1 y.o	Frozen	
Joint#5	M	1 y.o	Frozen	
Joint#6	M	1 y.o	Frozen	
Joint#7	M	1 y.o	Frozen	Collagen Diameter Measurement + Healthy
Joint#8	M	1 y.o	Frozen	
Joint#9	M	1 y.o	Frozen	
Joint#10	M	1 y.o	Frozen	

Figure 4. Experimental design and procedure for ACL extraction and characterization

2.1 Materials

The following materials were used in this research and were procured from Sigma-Aldrich: pyridine (#270970), 2.5% of glutaraldehyde solution (#G5882), phosphate buffer solution (#P5244), 1% osmium tetroxide (#75633), ethanol (#E7023), propylene oxide (#82320), epoxy embedding medium 812 substitute (#45345), epoxy embedding hardener DDSA (#45346), epoxy medium accelerator DMP 30 (#45348), epoxy embedding hardener MNA (#45347), acetic acid (#695092), polycaprolactone MW = 80000 g/mol (#440744), formic acid (#1.10854).

2.2 Harvesting the ACL tissue

The native sheep ACL tissues were harvested from the sheep knee joints obtained from a local slaughterhouse (n=10), kept at -20°C and examined for collagen fibril diameter and biomechanical properties. Before use, the frozen specimens were thawed at room temperature and characterized. All non-essential tissues such as muscles, fats and tendons other than ACL were removed with surgical blades (Sigma Aldrich, #S2646) attached to the handle (Sigma Aldrich, #S2896). Extraction of ACL tissue requires careful operation to keep the musculoskeletal structure of the sheep limb undamaged [62]. More information about the specimens is provided in Figure 4B.

2.3 Transmission Electron Microscopy

Transmission Electron Microscopy (TEM) is a microscope that can directly bombard a beam of electrons trespassing the ultra-thin sample as it passes through it. Healthy ACL specimens (n=4) were extracted from the medial region of ACL tissue to prepare TEM samples with the sizes of 1mm×1mm for preparation for imaging (Fig. 4C).

The process of sample preparation comprises several steps: fixation with chemicals, rinsing, secondary fixation, dehydration, infiltration, polishing, cutting and imaging.

The first step is the fixation of the specimen in the solution of 2.5% of glutaraldehyde (Sigma-Aldrich, #G5882) to prevent the changes and deformation of cell morphology and tissue decomposition. The specimens were placed in microtubes (Fisher, #05-408-129) containing 2.5% (Fig. 4D) glutaraldehyde solution and were placed in refrigerator for gradual cooling to 4°C. The process of cooling is required for the prevention of specimen deformation such as shrinkage or warping. The next procedure is the rinsing of specimens with phosphate buffer solution (Sigma-Aldrich, #P5244) three times for 10 minutes. Additional fixation comes with 1% osmium tetroxide (Sigma-Aldrich, #75633) for 2 hours. In addition, osmium tetroxide is utilized as a staining agent for electron microscopy. After second fixation, the samples were rinsed with PBS solution two times for 10 minutes each. Finally the specimens were treated with ethanol (Sigma-Aldrich, #E7023) and propylene oxide (Sigma-Aldrich, #82320) as described below:

1) Dehydration of the sample with 50% of ethanol for 40 minutes
2) Dehydration of the sample with 70% of ethanol for 12 hours
3) Dehydration of the sample with 96% of ethanol two times for 20 minutes

4) Dehydration of the sample with 100% of ethanol two times for 15 minutes
5) Dehydration of the sample with mixture of ethanol and propylene oxide two times for 10 minutes
6) Dehydration of the sample with propylene oxide two times for 15 minutes

This process of gradual dehydration is required to preserve the morphological structure of tissue.

The dehydrated specimens were, then, saturated with propylene oxide and resins with different concentrations. The resin is the mixture of epoxy compounds including 812 substitute (Sigma-Aldrich, #45345), DDSA (Sigma Aldrich, #45346), MNA (Sigma-Aldrich, #45347) and DMP 30 (Sigma-Aldrich, #45348). Samples were placed into the mixture of resin and propylene oxide (1:1) for 2 hours at 37℃. The mixture was then changed to 3:1 proportion for 2 hours, followed by pure resin for 12 hours. The embedded samples were polymerized for two days at 60℃. The resin hardened samples were cut in thin films using a microtome (Boeckeler RMC Power Tome Ultramicrotome, USA).

Finally, Transmission Electron Microscope (JEOL JEM-1400 Plus 120kV TEM, USA) is used for acquiring the images of ACL segments with high resolution and magnification (Fig. 4F). The longitudinal dissection was adjusted in molded capsules to observe the fibrils in cross sectional view. Imaging provided about 5-10 sections for each sample. Overall, 15-30 sections were imaged for each group of injured and healthy ACL tissues.

2.4 Measurements of fibril diameter

The images were edited via GIMP 2.10 (GIMP Development Team, USA) to add ten parallel lines with equal distances and only the fibers intersecting the lines were included in measurement. This method was used in previous studies to measure the diameter of native collagen fibrils and scaffold fibers [25,26]. Measurement of fibril diameters was done via ImageJ (National Institute of Health, USA) software. About 110 measurements were performed for each image. The same procedure was also used to evaluate the fiber diameters of PCL scaffolds.

2.5 Producing the nanosized scaffolds via electrospinning method

Polycaprolactone MW = 80000 g/mol (Sigma-Aldrich, ##440744) was used for scaffold fabrication. PCL solutions with different concentrations were prepared for

electrospinning method. For unimodal distributions, a total of 0.5 g of PCL was dissolved in the solution of acetic acid (#270725) and formic acid (90%, #110854) with 1% of pyridine (0.05mL) to get a final volume of 5 ml. The PCL solutions for bimodal fiber distribution were prepared using 0.2g and 0.375g PCL, in addition 0.015mL and 0.05 ml of pyridine respectively with formic and acetic acids in a total volume 5 ml. Solutions were prepared by mixing the ingredients for 2 hours with stirring at 1500 rpm at 40°C.

Co-electrospinning method was used for the fabrication of aligned nanosized fibers with bimodal distribution (Fig.5). PCL concentrations were 8% and 15%. The solutions were loaded into two oppositely positioned syringes and were directed to the drum collector. The voltage power source was set to 9 kV and the drum rotated at 2000 rpm. Moreover, the distance between needle tip and drum collector was set to 7 cm. The unaligned fibers were fabricated with solution of 11% PCL with flow rate of 0.03 mL/h at 9kV on a stationary plate (Fig.6).

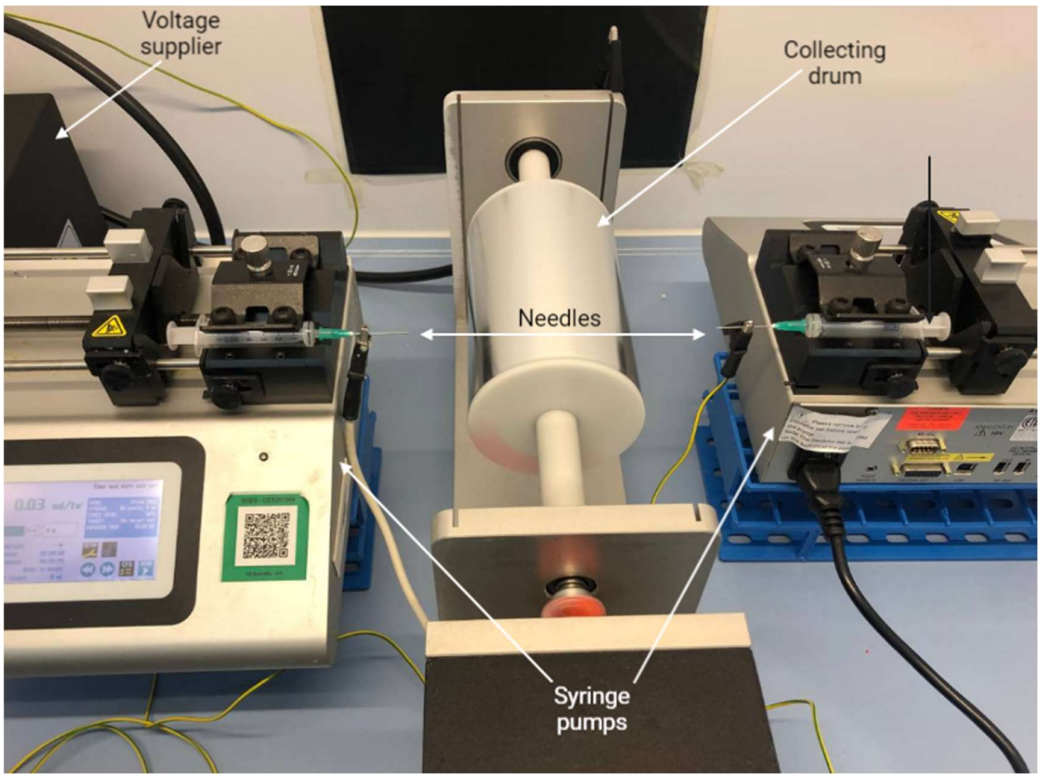

Figure 5. Electrospinning setup for aligned scaffold fabrication

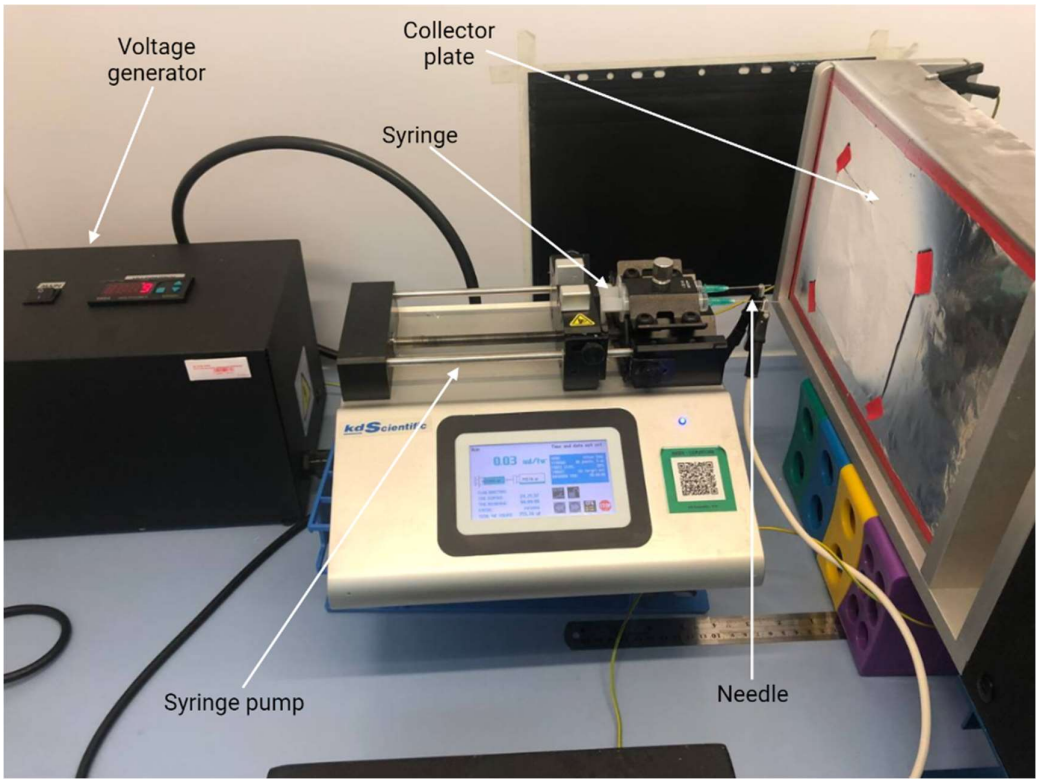

Figure 6. Electrospinning setup for unaligned scaffold fabrication

2.6 Mechanical properties and injured ACL creation

The injured ACLs were created by straining the healthy tissues to rupture using a uniaxial universal tension machine (Tinius Olsen H25KS, Horsham, PA, USA). Femur-ACL-tibia complex (FATC) was fixed in custom made two jaw-grips. Specimens (n=5/group) were preload at 4N and then extended at a crosshead speed of 5 mm/min up to failure. Meanwhile, stress-strain charts were registered by the mechanical testing device. A total of seven FATC were utilized for biomechanical testing. The region where ACL tissue ruptured was collected for TEM analysis to represent injured ACL.

Identical tensile tests were performed for PCL scaffolds via uniaxial universal mechanical testing device (MTS Criterion Model 43, MTS Systems Co., Eden Prairie, MN, USA). PCL scaffolds (n=5/group) with dimensions of 5cmx1cm (length x width) were fixed with custom-made grips and strained at a cross-head speed of 5 mm/min with 0.01 N preloading.

2.7 Scanning Electron Microscopy (SEM) and scaffold characterization

A turbo-pumped sputter coater (Quotrum Q150T ES, UK) was used for coasting the specimens with 3-5 nm thickness of gold layering at a current of 20mA. The scaffolds were then observed using an SEM (JSM-IT200(LA), JEOL, Japan) at various magnifications.

Measurement of scaffold fiber diameters was performed using ImageJ (National Institute of Health, USA) software. The fiber diameter distribution of unaligned scaffolds and aligned bimodal scaffolds were measured using at least 150 fibers per image (n=4 image/group).

2.8 Statistical analyses

Unpaired student-t test was utilized for analyzing and comparison of:

I. Collagen diameter of Healthy and injured ACL tissues.
II. Fiber diameter of PCL scaffold.
III. Mechanical properties of aligned and unaligned scaffolds.

One-way analysis of variance (ANOVA) was used for comparison ACL tissue and electrospun scaffolds for mechanical properties. The difference was considered significant for $p<0.05$.

3. Results

3.1 ACL fibril diameter

The collagen fibril diameters of healthy and injured ACL tissue are given in Figure 7. The respective TEM images are also depicted next to the histograms. Apparently, healthy specimens exhibit a bimodal distribution while the injured ACL tissue has a unimodal distribution. In addition, the healthy specimens had an organized structure with aligned collagen fibrils in the longitudinal direction (Fig. 7 A1, A2, A3, A4). The form of fibrils is circular. Oppositely, TEM photos of injured specimens exhibit an unaligned organization as indicated by the fibrils oriented in different directions.

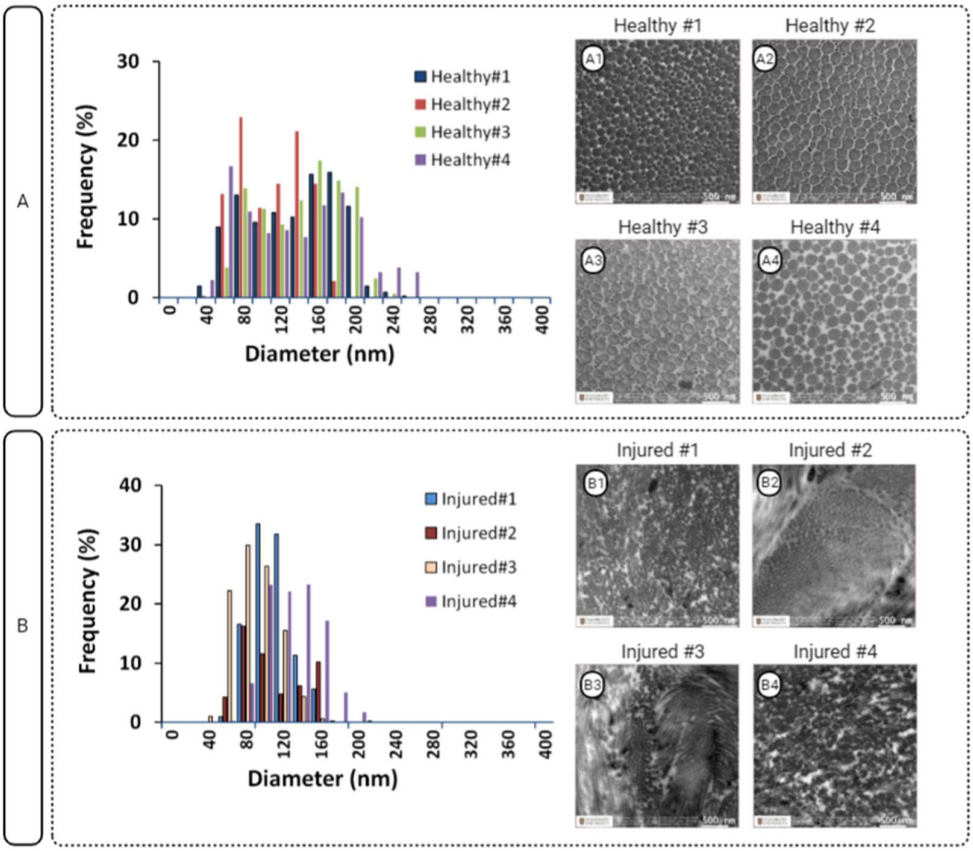

Figure 7. Healthy (A) and injured (B) diameter distribution of native ACL fibrils and TEM images (A1-A4, B1-B4). A1 - A4 are referred to the healthy ACL tissue specimens. B1 - B4 are referred to the injured ACL tissue specimens.

Combined distributions of injured and healthy ACL fibrils are demonstrated in Figure 8. The injured ACL tissue demonstrated a unimodal distribution with one peak at

101 ± 9.1 nm while the healthy ACL tissue had two peaks at 75.6 ± 8.5 nm and 157 ± 3.8 nm. The range of fibril diameter decreased from 24 – 291 nm to 36 – 230 nm, with the average value decreasing from 124.2 ± 16.1 to 86.2 ± 12.7 nm ($p < 0.05$, Fig. 8C). Moreover, the weighted mean diameter also reduced from 131.8 nm to 96.6 nm. Overall, the diameter of collagen fibrils of sheep ACL changed from a bimodal to a unimodal distribution after the injury, with a reduced mean diameter.

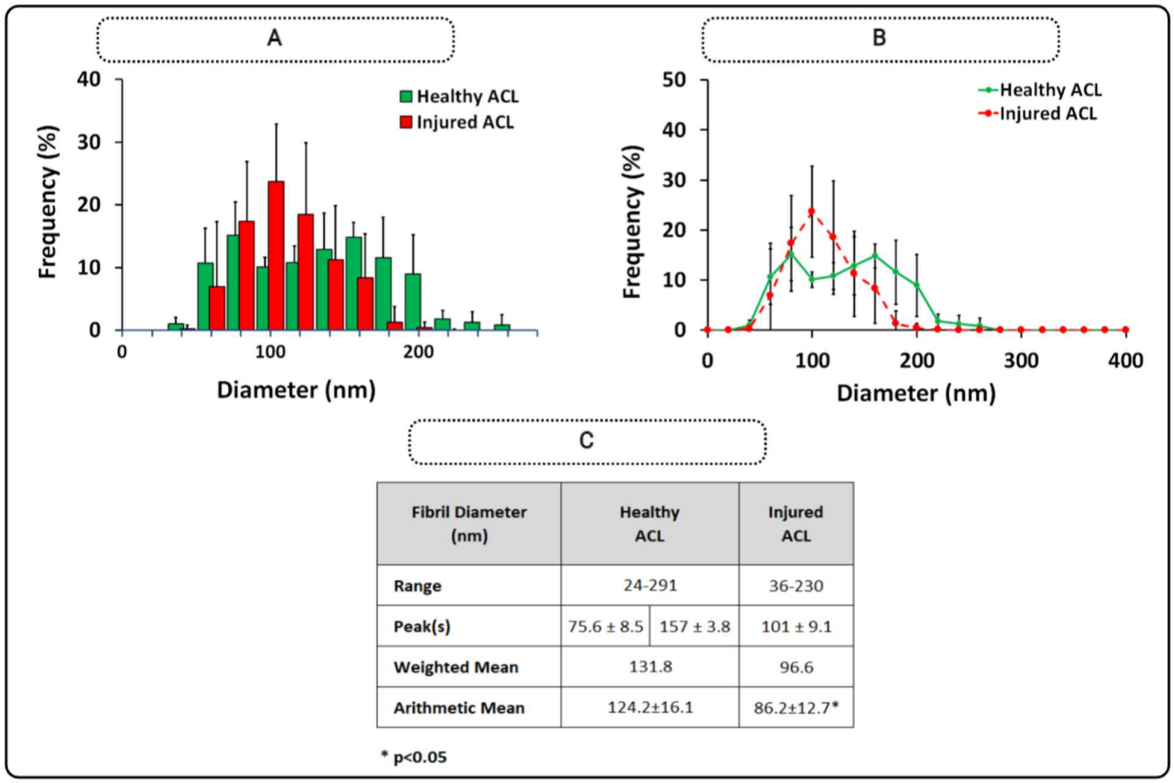

Fibril Diameter (nm)	Healthy ACL		Injured ACL
Range	24-291		36-230
Peak(s)	75.6 ± 8.5	157 ± 3.8	101 ± 9.1
Weighted Mean	131.8		96.6
Arithmetic Mean	124.2±16.1		86.2±12.7*

Figure 8. Compared injured and healthy diameter distributions in the histogram (A) and line graph charts (B) with definitive statistics (C). * corresponds to statistical difference at $p<0.05$ (n=4) and standard deviation is exposed as error bars.

3.2 Fiber diameter of PCL scaffolds

Histograms of aligned and unaligned PCL scaffolds are given in Figure 9, together with their SEM images. Obviously, the aligned scaffolds demonstrated a bimodal distribution. The unaligned (random) scaffolds showed a unimodal distribution.

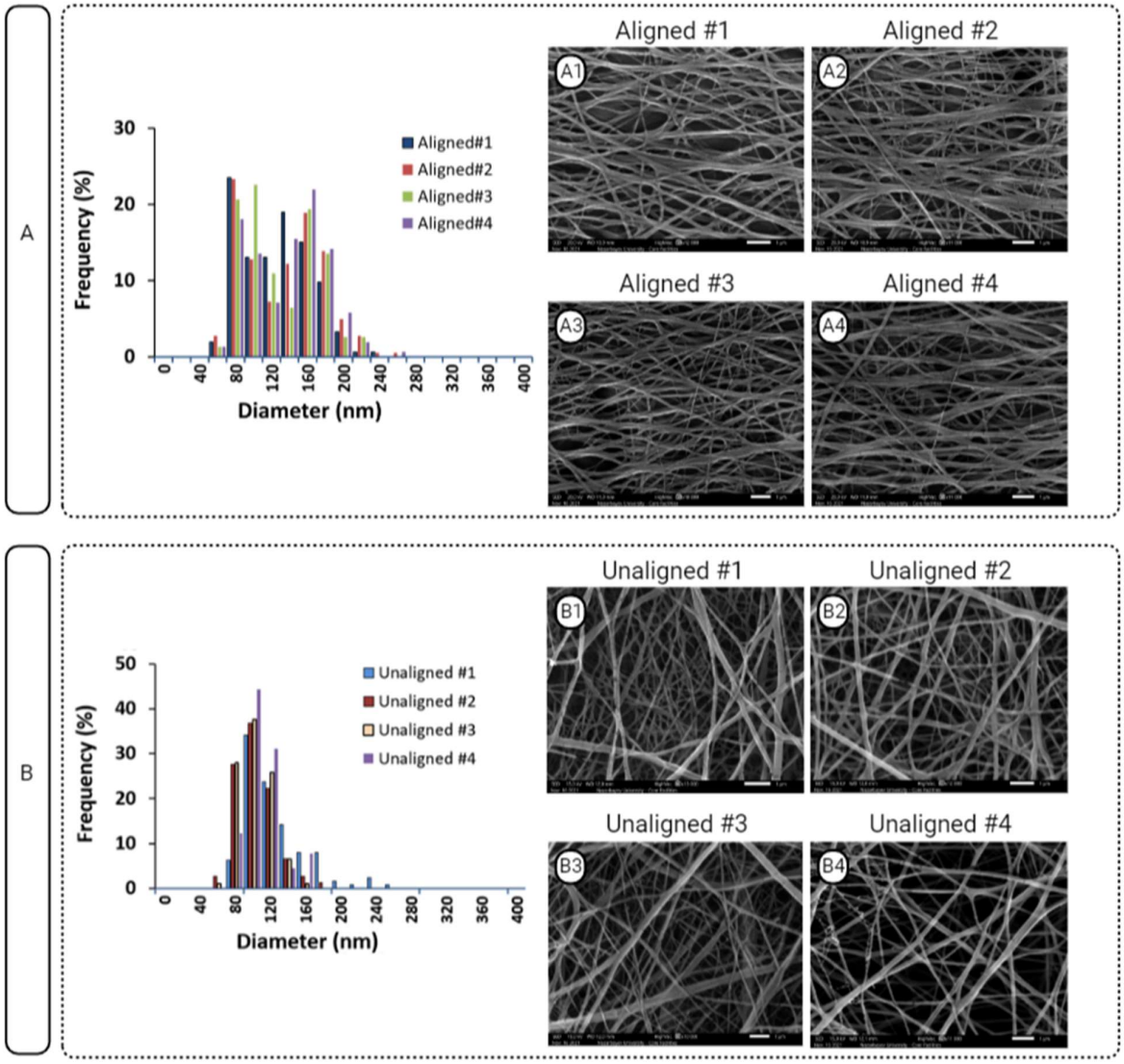

Figure 9. Diameter distribution of (A) aligned and (B) unaligned PCL fibers and corresponding (A1 - 4 and B1 - 4) SEM images. Individual specimens derived from aligned PCL scaffolds (n=4) are referred to as A1 - A4 Individual specimens obtained from unaligned PCL scaffolds (n=4) are referred to as B1 – B4. Scale bar = 1μm.

Figure 10 illustrates the combined fiber diameter distribution for aligned and unaligned PCL scaffolds. Clearly, unaligned PCL scaffolds displayed a distribution with one peak at 101.5 ± 15.4 nm, whereas aligned scaffolds exhibited two peaks at 85 ± 10nm and 155 ± 10 nm. The average fiber diameter decreased from 122.1 ± 5.9 nm to 101.5 ± 15.4 nm ($p<0.05$, Figure 10C) and the range of PCL fiber diameter changed from 47- 262 nm to 42- 263 nm. The mean diameter of frequency weighted fibers decreased from 131.2nm to 110.8 nm.

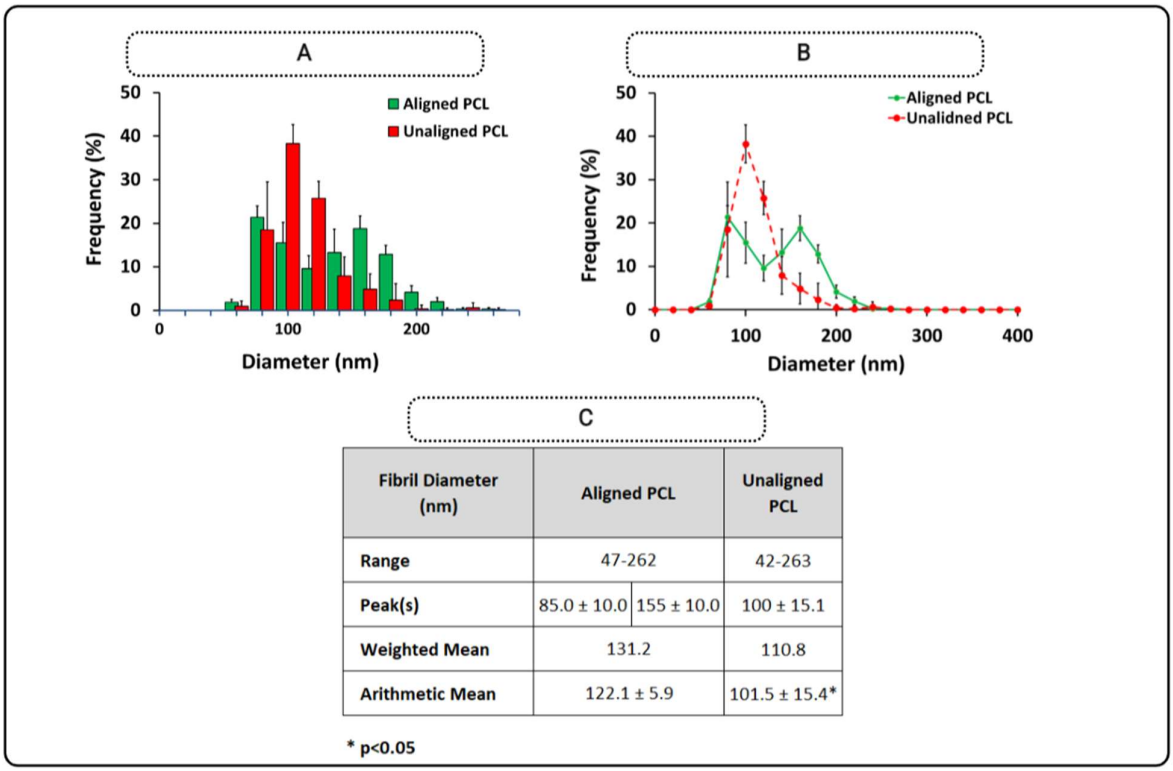

C

Fibril Diameter (nm)	Aligned PCL		Unaligned PCL
Range	47-262		42-263
Peak(s)	85.0 ± 10.0	155 ± 10.0	100 ± 15.1
Weighted Mean	131.2		110.8
Arithmetic Mean	122.1 ± 5.9		101.5 ± 15.4*

* p<0.05

Figure 10. United aligned and unaligned PCL fiber diameter distributions in the form of (A) histogram and (B) line graph, along with (C) descriptive statistics. * denotes a statistical difference at p<0.05 (n=4), while error bars denote standard deviation.

The fiber diameter distributions of aligned and unaligned PCL scaffold fibers are comparable to healthy and injured ACL tissue, respectively. Figure 11 and Figure 12 clearly demonstrate the similarity of diameters between native ACL tissue and electrospun scaffolds. No statistically significant difference was detected between the diameters of aligned PCL versus healthy ACL and unaligned PCL versus injured ACL as shown in Fig 11 and Fig 12.

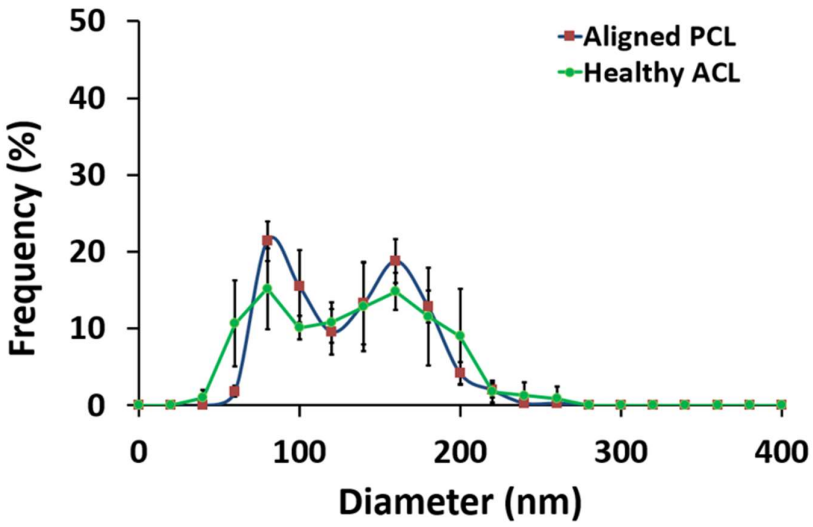

	Aligned PCL	Healthy ACL
Mean diameter, nm	122.1 ± 5.9	124.2 ± 16.1

Figure 11. Comparison of bimodal diameter distribution in line graphs between Aligned PCL and Healthy ACL

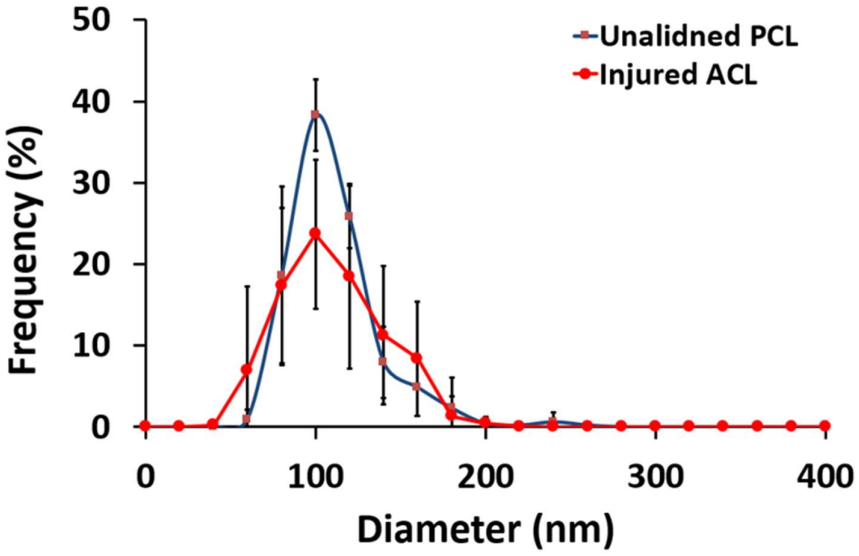

	Unaligned PCL	Injured ACL
Mean diameter, nm	101.5 ± 15.4	86.2 ± 12.7

Figure 12. Comparison of unimodal diameter distribution in line graphs between Unaligned PCL and Injured ACL

3.3 Biomechanical properties of ACL tissue and PCL scaffolds

Figure 13A depicts the load-elongation and stress-strain curves of healthy ACL tissue, with an initial toe area followed by a linear region, and lastly a yield region. The ACL tissue shows a normal tri-phase pattern. The ACL tissue has an ultimate stress and

strain of 23.1 ± 12.0 MPa and 42.9 ± 24.6%, respectively. According to the linear portion of the stress-strain curve, the tissue has a modulus of 0.5 ± 0.2 MPa. The strain energy density, defined as the area under the curve describing the energy acquired by stressing the material, was determined to be 600.3 ± 466.2MPa. The ACL was strained to an ultimate load of 568.7 ± 213.6 N with an elongation of 8.7± 3.3 mm (Figure 13A).

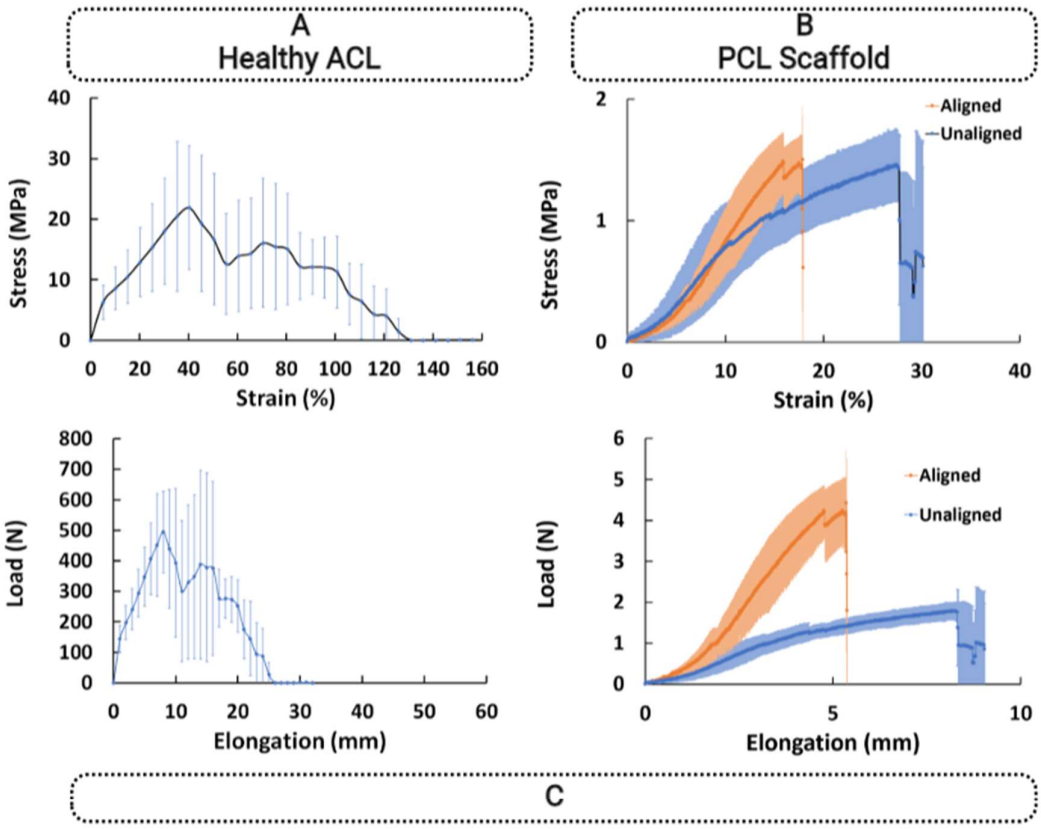

	Ultimate Stress (MPa)	Ultimate Strain (%)	Strain at Break (%)	Modulus (MPa)	Strain Energy Density (MPa)	Ultimate Load (N)	Ultimate Strain (mm)
ACL	23.1 ± 12.0	42.9 ± 24.6	133.1 ± 59.8	0.5± 0.2	600.3 ± 466.2	568.7 ± 213.6	8.7 ± 3.3
PCL Unaligned	1.5 ± 0.3 *	26.7 ± 1.8 *	28.5 ± 3.5 *	0.11 ± 0.03 *	2.7 ± 0.5 *	1.8 ± 0.2 *	8.0 ± 0.6 *
PCL Aligned	1.7 ± 0.11 *	20.3 ± 6.5 *	21.1 ±6.5 *	0.1 ± 0.04 *	4.1 ± 0.9 *	4.9 ± 0.49 *	6.1 ± 1.95 *

* indicates difference between groups at p<0.05

Figure 13. Native ACL tissue and PCL scaffold mechanical performance. (A) Native ACL tissue, (B) electrospun PCL scaffolds with bimodal and unimodal fiber diameter distributions, respectively, and (C) descriptive statistics of PCL scaffolds. * indicates significant difference at p<0.05. Error bars represent SD.

Figure 13B depicts the PCL scaffolds' load-elongation and stress-strain curves. The PCL scaffolds had a typical tri-phasic tensile pattern such as toe, linear and yield regions. Figure 13C displays the results for the common mechanical performance parameters of PCL scaffolds. The aligned PCL scaffolds representing healthy ACL tissue

were found to have ultimate stress and strain of 1.7 ± 0.11 MPa and 20.3 ± 6.5%, respectively. Likewise, the ultimate stress and ultimate strain of the unaligned PCL scaffolds, representing the injured ACL tissue, were of 1.5 ± 0.3 MPa and 26.7 ± 1.8%, respectively.

The moduli of the aligned and unaligned scaffolds were 0.1 ± 0.04 MPa and 0.11 ± 0.03 MPa, respectively. For aligned and unaligned scaffolds, the strain energy density was determined to be 4.1 ± 0.9 MPa and 2.7 ± 0.5 MPa, respectively. The ultimate tensile load of the two types of scaffolds such as aligned and unaligned was 4.9 ± 0.49 N and 1.8 ± 0.2 N when stretched to an elongation of 6.1 ± 1.95 mm and 8.0 ± 0.6 mm, respectively.

In terms of mechanical characteristics, an evaluation of the aligned/unaligned scaffolds and natural ACL tissue (Figure 13C and Figure 14) confirmed that the results for all parameters were significantly lower than the native ACL tissue.

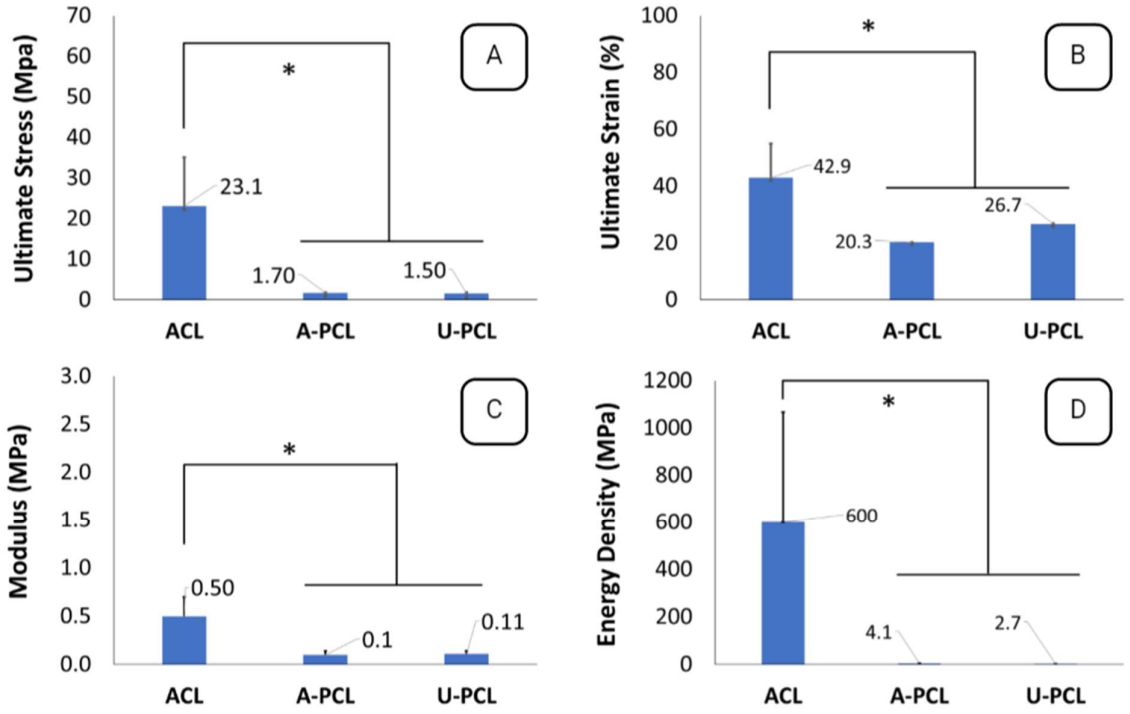

Figure 14. An evaluation of native ACL and electrospun scaffolds in terms of mechanical properties (A: ultimate stress, B: ultimate strain, C: modulus, D: energy density). * displays essential difference at $p<0.05$. A-PCL: Aligned PCL, U-PCL: Unaligned PCL.

Discussion

The means and distributions of collagen fibril diameter of sheep ACL before and after injury as well as the tensile properties of healthy ACL tissue were studied in this thesis research. Furthermore, tensile properties and the fiber diameter distribution of electrospun PCL scaffolds were assessed to validate the biomimicry of the PCL scaffolds. The collagen fibril diameter distribution of sheep ACL changed from bimodal to unimodal after rupture, with a reduction in mean diameter. Furthermore, the fiber diameter distribution of PCL electrospun scaffold demonstrated bimodal and unimodal distribution behavior to qualitatively and quantitatively replicate the healthy and injured ACL tissues.

The structural and biological properties of ACL tissue are closely connected to its function. ACL collagen fibers are structured in bundles of fibrils in a parallel wave pattern along the longitudinal axis as shown in TEM images. This structure improves the mechanical properties of ACL [38]. Our results revealed that a healthy sheep ACL tissue has a well-organized/aligned pattern of collagen fibrils, which is disrupted when the tissue is injured. Completely ruptured human ACLs and rat patellar tendon were shown to have a similar disorganized collagen fibril configuration [39, [63]. Our observations on the organizational variation in sheep ACL collagen fibrils following rupture obviously contributes to the existing research in this field.

The reduction in average collagen fibril diameter and a transition in fibril diameter distribution from bimodal to unimodal distribution are characteristics of tendon/ligament tissues. Bovine ACL [30], rabbit MCL [64], human ACL [39], mouse/rat PT [31, 60] all previously demonstrated structural variation upon injury. Previous research performed on bovine ACL [65] showed diameter peaks of ~100 and 250 nm before injury that shifted to a single peak of 100 nm. Similarly, the collagen fibril diameter of human ACL [66] with an average diameter of 75 nm (20-185 nm) changed to 71 nm (20-290) nm. This thesis research evaluated collagen fibril diameter distribution of healthy and injured sheep ACL. Results showed that the mean diameter of fibrils decreased significantly after the mechanical injury, with a change of modality from bimodal to unimodal. Research group of Rumian [37] reported the results of mean collagen fibril diameter of 3 year healthy ovine as 181±14 nm having a bimodal distribution with peaks of 60 and 200 nm. This is the only relevant study for the sheep and ovine ACL models found in literature, and in comparison with our results the main difference is that the sheep model in this thesis

research is the immature animal of one year old. The mean diameter of the collagen fibrils and the diameter range of the sheep ACL model in healthy and injured states were measured as124 ± 16.1 nm and 86 ± 12.7 nm, respectively, in this thesis research.

The published research for tendon/ligament tissues from various species, such as ACLs of human, bovine and rabbit, FT and AT of mouse only provided the average fibril diameters and diameter ranges of healthy tissues without mentioning the distribution of fibril diameter after injury [35, 37, 62, 33, 61, 29]. One exception is the study performed by our group using bovine ACL tissue [30]. As a result, the current research investigated the collagen fibril diameter distribution in sheep ACL with and without injury. The findings demonstrated that after injury, the average fibril diameter decreased, indicating a transition in fibril diameter modality from bimodal to unimodal. The results of the work performed by Beisbayeva et al on bovine ACL tissue and our results for sheep ACL tissue are comparable in terms of diameter distribution. More specifically, the mean peak fibril diameters of the healthy bovine ACL tissue were 73.3±11.5 nm and 213±11.5nm as compared to 75.6 ± 8.5 nm and 157.6 ± 3.8 nm, respectively, for sheep ACL in this study.

PCL electrospun scaffolds were produced via electrospinning technique to represent the healthy and injured states of sheep ACL tissues. The aligned and unaligned PCL scaffolds represented the collagen fibril diameter distribution of healthy and injured ACL. Both qualitatively and quantitatively, PCL scaffolds with aligned and unaligned structures mimicked the ACL collagen fibrils in healthy and injured states. For instance, the average diameter of aligned PCL scaffolds and healthy ACL were found as 122.1 ± 5.9 nm and 124 ± 16.1 nm, respectively. Similarly, the average diameter of unaligned PCL scaffold (101.5 ± 15.4 nm) and injured ACL (86 ± 12.7 nm) were not different. Although electrospinning method is suitable for producing nanosized scaffolds, it has limitations including difficulty to fabricate fibers with constant diameter as well existence of cracks if the processing and material properties are not properly tuned [68].

The mean diameter and distribution of collagen fibrils of ACL are the major indicators of tissue mechanics and any alterations in fibril diameter and distribution were shown to have a direct impact on mechanical properties [35, 15, 63]. Because the interfibrillar gaps between thicker fibrils are filled with thinner fibrils to produce a highly packed ECM configuration, a bimodal distribution, as exhibited in healthy ACL tissue, leads to higher mechanical properties. When this hierarchical structure is disrupted, ligament tissue's ability to resist physiologic stress is reduced, making the tissue mechanically vulnerable. It should be noted that only the mechanical characteristics of

healthy ACL tissue were examined in this work. Tensile testing demonstrated that when stretched by 42.9 ± 24.6%, healthy sheep ACL tissue could withstand a load of 600.3 ± 466.2N. The literature on the tensile characteristics of sheep ACL is limited. Unfortunately, there is no research on the physiologic level strain rates for sheep ACL tissue. In this study, we chose a deformation of 5mm/min based on our past experience [22] and the available literature data.

The native ACL tissue outperformed both aligned and unaligned PCL scaffolds in every parameter measured in this study, including ultimate strain, ultimate stress, strain energy density and modulus. The aligned PCL scaffolds outperformed their unaligned counterparts in maximum load, whereas the unaligned scaffold revealed the larger value of strain, according to a comparison within the two scaffold groups, which is consistent with previously reported data for the tensile characteristics of aligned and unaligned PCL scaffolds. [27, 64, 65].

There are some methodological limitations in this research study. For instance, due to a lack of appropriate apparatus, the mechanical characteristics of injured ACL could not be assessed. Such a measurement would allow for the comparison of unaligned PCL scaffolds and damaged ACL tissue. Furthermore, the mechanical properties of ACL tissue were investigated in this report by implementing a tensile stress to the FATC, despite the fact that biomechanics in the sagittal plane is the major cause of ACL stress [72].

4. Conclusion

This research study examined the structural and mechanical properties of native sheep ACL before and after injury. Electrospinning was used to create nanofiber scaffolds to mimic the structural characteristics of both healthy and damaged ACL tissues. The distribution of fibril diameter of sheep ACL altered from bimodal to unimodal after rupture, with a decrease in average diameter. The bimodal and unimodal fiber diameter distributions of PCL scaffold represented the cases of healthy and damaged ACL tissues, respectively. In comparison to PCL scaffolds, the ACL tissue demonstrated improved mechanical characteristics. To the best of our knowledge, currently no report exists on the production and use of electrospun nanofibers with bimodal distribution for ACL reconstruction/regeneration. This scaffold design differs from the frequently utilized unimodal scaffolds. In conclusion, the results of this study are expected to have a substantial influence on the orthopedic research society's attempts.

Reference list

[1] W. L. Lim, L. L. Liau, M. H. Ng, S. R. Chowdhury, and J. X. Law, “Current Progress in Tendon and Ligament Tissue Engineering,” *Tissue Eng. Regen. Med.*, vol. 16, no. 6, p. 549, Dec. 2019.

[2] D. Zbrojkiewicz, C. Vertullo, and J. E. Grayson, “Increasing rates of anterior cruciate ligament reconstruction in young Australians, 2000–2015,” *Med. J. Aust.*, vol. 208, no. 8, pp. 354–358, Apr. 2018.

[3] S. G. F. Abram, A. Judge, D. J. Beard, and A. J. Price, “Rates of Adverse Outcomes and Revision Surgery After Anterior Cruciate Ligament Reconstruction: A Study of 104,255 Procedures Using the National Hospital Episode Statistics Database for England, UK,” *Am. J. Sports Med.*, vol. 47, no. 11, pp. 2533–2542, Sep. 2019.

[4] J. M. Hootman, R. Dick, and J. Agel, “by the National Athletic Trainers,” Association, Inc, 2007.

[5] C. Zhang, J. Zhu, Y. Zhou, B. P. Thampatty, and J. H.-C. Wang, “Tendon Stem/Progenitor Cells and Their Interactions with Extracellular Matrix and Mechanical Loading,” *Stem Cells Int.*, vol. 2019, pp. 1–10, Oct. 2019.

[6] H. J. Silvers and B. R. Mandelbaum, “ACL Injury Prevention in the Athlete,” *Sport. - Sport.*, vol. 27, no. 1, pp. 18–26, Jan. 2011.

[7] A. A. Macaulay, D. C. Perfetti, and W. N. Levine, “Anterior cruciate ligament graft choices,” *Sports Health*, vol. 4, no. 1, pp. 63–68, Jan. 2012.

[8] J. Anjana, S. Deepthi, K. T. Shalumon, U. Mony, J. P. Chen, and R. Jayakumar, “Nanoengineered biomaterials for tendon/ligament regeneration,” in *Nanoengineered Biomaterials for Regenerative Medicine*, Elsevier, 2018, pp. 73–93.

[9] M. Benjamin, E. J. Evans, and L. Copp, “The histology of tendon attachments to bone in man.,” *J. Anat.*, vol. 149, p. 89, Dec. 1986.

[10] I.-N. E. Wang, S. Mitroo, F. H. Chen, H. H. Lu, and S. B. Doty, “Age-dependent changes in matrix composition and organization at the ligament-to-bone insertion,” *J. Orthop. Res.*, vol. 24, no. 8, pp. 1745–1755, Aug. 2006.

[11] M. J. Friedman, O. H. Sherman, J. M. Fox, W. Del Pizzo, S. J. Snyder, and R. J. Ferkel, “Autogeneic anterior cruciate ligament (ACL) anterior reconstruction of the knee. A review.,” *Clin. Orthop. Relat. Res.*, vol. NO. 196, no. 196, pp. 9–14, Jun. 1985.

[12] D. B. Robertson, D. M. Daniel, and E. Biden, “Soft tissue fixation to bone,” *Am. J. Sports Med.*, vol. 14, no. 5, pp. 398–403, Apr. 1986.

[13] C. B. Frank, “Ligament structure, physiology and function,” *J. Musculoskelet. Neuronal Interact.*, vol. 4(2), pp. 199–201, 2004.

[14] V. B. Duthon, C. Barea, S. Abrassart, J. H. Fasel, D. Fritschy, and J. Ménétrey, “Anatomy of the anterior cruciate ligament,” *Knee Surgery, Sports Traumatology, Arthroscopy*, vol. 14, no. 3. Springer, pp. 204–213, 19-Mar-2006.

[15] M. Marieswaran, I. Jain, B. Garg, V. Sharma, and D. Kalyanasundaram, “A review on biomechanics of anterior cruciate ligament and materials for reconstruction,” *Appl. Bionics Biomech.*, vol. 2018, 2018.

[16] J. Kastelic, A. Galeski, and E. Baer, “The multicomposite structure of tendon,” *Connect. Tissue Res.*, vol. 6, no. 1, pp. 11–23, 1978.

[17] H. Fujie, “Mechanical properties and biomechanical function of the ACL,” in *ACL Injury and its Treatment*, Tokyo: Springer Japan, 2016, pp. 69–77.

[18] D. J. Dos Santos, D. J. Carastan, L. B. Tavares, and G. F. Batalha, “Polymeric Materials Characterization and Modeling,” *Compr. Mater. Process.*, vol. 2, pp. 37–63, Jan. 2014.

[19] H. Belyadi, E. Fathi, and F. Belyadi, “Rock mechanical properties and in situ stresses,” *Hydraul. Fract. Unconv. Reserv.*, pp. 215–231, Jan. 2019.

[20] P. B. Bartolin, R. Boixadera, and D. Hudetz, “Experimental testing and finite element method analysis of the anterior cruciate ligament primary repair with internal brace augmentation,” *Med. Eng. Phys.*, vol. 95, pp. 76–83, Sep. 2021.

[21] K. Ohtera *et al.*, “Effect of pregnancy on joint contracture in the rat knee,” *J. Appl. Physiol.*, vol. 92, no. 4, pp. 1494–1498, 2002.

[22] A. C. Gurlek, B. Sevinc, E. Bayrak, and C. Erisken, “Synthesis and characterization of polycaprolactone for anterior cruciate ligament regeneration,” *Mater. Sci. Eng. C*, vol. 71, pp. 820–826, Feb. 2017.

[23] R. Meller *et al.*, “Histologic and Biomechanical Analysis of Anterior Cruciate Ligament Graft to Bone Healing in Skeletally Immature Sheep,” *Arthrosc. J. Arthrosc. Relat. Surg.*, vol. 24, no. 11, pp. 1221–1231, Nov. 2008.

[24] A. Weiler, R. Peine, A. Pashmineh-Azar, C. Abel, N. P. Südkamp, and R. F. G. Hoffmann, “Tendon healing in a bone tunnel. Part I: Biomechanical results after biodegradable interference fit fixation in a model of anterior cruciate ligament reconstruction in sheep,” *Arthrosc. J. Arthrosc. Relat. Surg.*, vol. 18, no. 2, pp. 113–123, Feb. 2002.

[25] C. Rodríguez, Tomás, E. García, S. Montes, Luis Rodríguez, and A. Maestro, “In vitro comparison between cortical and cortico-cancellous femoral suspension devices for anterior cruciate ligament reconstruction: implications for mobilization,” *Vitr. Comp. between cortical cortico-cancellous femoral Suspens. devices anterior cruciate ligament Reconstr. Implic. mobilization*, vol. 23, no. 8, 2015.

[26] S. L. Y. Woo, J. M. Hollis, D. J. Adams, R. M. Lyon, and S. Takai, “Tensile properties of the human femur-anterior cruciate ligament-tibia complex: The effects of specimen age and orientation,” *Am. J. Sports Med.*, vol. 19, no. 3, pp. 217–225, Apr. 1991.

[27] L. Diotalevi, Y. Petit, V. Brailovski, S. Nichols, E. Marchionatti, and É. Wagnac, “Quasi-static tensile properties of the Cranial Cruciate Ligament (CrCL) in adult cattle: towards the design of a prosthetic CrCL,” *J. Mech. Behav. Biomed. Mater.*, vol. 79, pp. 239–245, Mar. 2018.

[28] M. Torre *et al.*, “ACL reconstruction by bone-patellar tendon-bone graft: mechanical evaluation of the elastic modulus and failure modes,” *J Orthopaed Traumatol*, vol. 4, pp. 69–75, 2003.

[29] A. J. Niehaus, D. E. Anderson, J. K. Johnson, and J. J. Lannutti, “Comparison of the mechanical characteristics of polymerized caprolactam and monofilament nylon loops constructed in parallel strands or as braided ropes versus cranial cruciate ligaments of cattle,” *Am. J. Vet. Res.*, vol. 74, no. 3, pp. 381–385, Mar. 2013.

[30] Z. Beisbayeva, A. Zhanbassynova, G. Kulzhanova, F. Mukasheva, and C. Erisken, “Change in Collagen Fibril Diameter Distribution of Bovine Anterior Cruciate Ligament upon Injury Can Be Mimicked in a Nanostructured Scaffold,” *Molecules*, vol. 26, no. 5, p. 1204, Feb. 2021.

[31] D. L. Butler, “Ligamentous Restraints to Anterior-Posterior Drawer in the Human Knee A BIOMECHANICAL STUDY,” 1992.

[32] R. Gehwolf *et al.*, “Pleiotropic roles of the matricellular protein Sparc in tendon maturation and ageing,” *Sci. Reports 2016 61*, vol. 6, no. 1, pp. 1–15, Sep. 2016.

[33] B. L. Proffen, M. McElfresh, B. C. Fleming, and M. M. Murray, “A COMPARATIVE ANATOMICAL STUDY OF THE HUMAN KNEE AND SIX ANIMAL SPECIES,” *Knee*, vol. 19, no. 4, p. 493, Aug. 2012.

[34] J. M. Johnston *et al.*, “Collagen V haploinsufficiency in a murine model of classic Ehlers–Danlos syndrome is associated with deficient structural and mechanical healing in tendons,” *J. Orthop. Res.*, vol. 35, no. 12, pp. 2707–2715, Dec. 2017.

[35] T. M. Evangelisches, K. Wien, and R. Schabus, “Article in Archives of Orthopaedic and Trauma Surgery,” 2001.

[36] R. A. Hart, W. H. Akeson, K. Spratt, and D. Amiel, “Collagen Fibril Diameter Distributions in Rabbit Anterior Cruciate and Medial Collateral Ligaments: Changes with Maturation,” *Iowa Orthop. J.*, vol. 19, p. 66, 1999.

[37] A. P. Rumian, A. L. Wallace, and H. L. Birch, “Tendons and ligaments are anatomically distinct but overlap in molecular and morphological features—a comparative study in an ovine model,” *J. Orthop. Res.*, vol. 25, no. 4, pp. 458–464, Apr. 2007.

[38] J. Zhu, X. Zhang, Y. Ma, C. Zhou, and yingfang Ao, “Ultrastructural and Morphological Characteristics of Human Anterior Cruciate Ligament and Hamstring Tendons,” *Anat. Rec. Adv. Integr. Anat. Evol. Biol.*, vol. 295, no. 9, pp. 1430–1436, Sep. 2012.

[39] M. Friedrich Neurath and E. Stofft, “Acta Orthopaedica Scandinavica Collagen ultrastructure in ruptured cruciate ligaments An electron microscopic

investigation," 2009.

[40] M. Ochi, T. Murao, Y. Sumen, K. Kobayashi, and N. Adachi, "Isolated Posterior Cruciate Ligament Insufficiency Induces Morphological Changes of Anterior Cruciate Ligament Collagen Fibrils," *Arthrosc. J. Arthrosc. Relat. Surg.*, vol. 15, no. 3, pp. 292–296, Apr. 1999.

[41] D. Qu *et al.*, "Micro-and Ultrastructural Characterization of Age-Related Changes at the Anterior Cruciate Ligament-to-Bone Insertion," 2016.

[42] F. J. O'Brien, "Biomaterials & scaffolds for tissue engineering," *Mater. Today*, vol. 14, no. 3, pp. 88–95, Mar. 2011.

[43] Q. L. Loh and C. Choong, "Three-Dimensional Scaffolds for Tissue Engineering Applications: Role of Porosity and Pore Size," *Tissue Eng. Part B. Rev.*, vol. 19, no. 6, p. 485, Dec. 2013.

[44] X. Zhang, D. Bogdanowicz, C. Erisken, N. M. Lee, and H. H. Lu, "Biomimetic Scaffold Design for Functional and Integrative Tendon Repair," *J. Shoulder Elb. Surg.*, vol. 21, no. 2, p. 266, Feb. 2012.

[45] E. Francois, D. Dorcemus, and S. Nukavarapu, "Biomaterials and scaffolds for musculoskeletal tissue engineering," *Regen. Eng. Musculoskelet. Tissues Interfaces*, pp. 3–23, Jan. 2015.

[46] S. Samavedi, P. Vaidya, P. Gaddam, A. R. Whittington, and A. S. Goldstein, "Electrospun meshes possessing region-wise differences in fiber orientation, diameter, chemistry and mechanical properties for engineering bone-ligament-bone tissues," *Biotechnol. Bioeng.*, vol. 111, no. 12, pp. 2549–2559, Dec. 2014.

[47] G. Criscenti *et al.*, "Triphasic scaffolds for the regeneration of the bone–ligament interface," *Biofabrication*, vol. 8, no. 1, p. 015009, Jan. 2016.

[48] N. Jiang, J. He, W. Zhang, D. Li, and Y. Lv, "Directed differentiation of BMSCs on structural/compositional gradient nanofibrous scaffolds for ligament-bone osteointegration," *Mater. Sci. Eng. C*, vol. 110, p. 110711, May 2020.

[49] J. He *et al.*, "Microfiber-reinforced nanofibrous scaffolds with structural and material gradients to mimic ligament-to-bone interface," *J. Mater. Chem. B*, vol. 5, no. 43, pp. 8579–8590, Nov. 2017.

[50] S. Samavedi, C. Olsen Horton, S. A. Guelcher, A. S. Goldstein, and A. R. Whittington, "Fabrication of a model continuously graded co-electrospun mesh for regeneration of the ligament–bone interface," *Acta Biomater.*, vol. 7, no. 12, pp. 4131–4138, Dec. 2011.

[51] S. Samavedi, S. A. Guelcher, A. S. Goldstein, and A. R. Whittington, "Response of bone marrow stromal cells to graded co-electrospun scaffolds and its implications for engineering the ligament-bone interface," *Biomaterials*, vol. 33, no. 31, pp. 7727–7735, Nov. 2012.

[52] M. V Robi K, Jakob N, Matevz K, "The physiology of sports injuries and repair processes," K. Y. Hamlin M, Draper N, Ed. London: InTech, 2013.

[53] T. Kano *et al.*, “Influence of the site of injury on the spontaneous healing response in a rat model of total rupture of the anterior cruciate ligament,” *Connect. Tissue Res.*, pp. 1–13, Mar. 2021.

[54] Z. Lin, “Osteogenic and tenogenic induction of hBMSCs by integrated nanofibrous scaffold with chemical and structural mimic to bone-ligament connection,” *Artic. J. Mater. Chem. B*, 2016.

[55] D. Olvera, B. N. Sathy, S. F. Carroll, and D. J. Kelly, “Modulating microfibrillar alignment and growth factor stimulation to regulate mesenchymal stem cell differentiation,” *Acta Biomater.*, vol. 64, pp. 148–160, Dec. 2017.

[56] D. Olvera, B. N. Sathy, and D. J. Kelly, “Spatial Presentation of Tissue-Specific Extracellular Matrix Components along Electrospun Scaffolds for Tissue Engineering the Bone–Ligament Interface,” *ACS Biomater. Sci. Eng.*, vol. 6, no. 9, pp. 5145–5161, Sep. 2020.

[57] S. Farah, D. G. Anderson, and R. Langer, “Physical and mechanical properties of PLA, and their functions in widespread applications — A comprehensive review,” *Advanced Drug Delivery Reviews*, vol. 107. Elsevier B.V., pp. 367–392, 15-Dec-2016.

[58] D. Gorth and T. J. Webster, “Matrices for tissue engineering and regenerative medicine,” 2011.

[59] C. Erisken, D. M. Kalyon, and H. Wang, “A hybrid twin screw extrusion/electrospinning method to process nanoparticle-incorporatedelectrospun nanofibres,” *Nanotechnology*, vol. 19, no. 16, p. 165302, Mar. 2008.

[60] A. Haider, S. Haider, and I. K. Kang, “A comprehensive review summarizing the effect of electrospinning parameters and potential applications of nanofibers in biomedical and biotechnology,” *Arab. J. Chem.*, vol. 11, no. 8, pp. 1165–1188, Dec. 2018.

[61] A. Sensini, G. Massafra, C. Gotti, A. Zucchelli, and L. Cristofolini, “Tissue Engineering for the Insertions of Tendons and Ligaments: An Overview of Electrospun Biomaterials and Structures,” *Front. Bioeng. Biotechnol.*, vol. 0, p. 98, Mar. 2021.

[62] C. F. Lindboe, T. O. Fjeld, and H. Steen, “Morphological changes in continuously stretched skeletal muscles in sheep,” *Eur. J. Appl. Physiol. Occup. Physiol.*, vol. 54, pp. 184–190, 1985.

[63] T. Muellner *et al.*, “Light and electron microscopic study of stress-shielding effects on rat patellar tendon,” *Arch. Orthop. Trauma Surg. 2001 12110*, vol. 121, no. 10, pp. 561–565, 2001.

[64] S. L. Y. Woo, Y. Takakura, R. Liang, F. Jia, and D. K. Moon, “Treatment with Bioscaffold Enhances the the Fibril Morphology and the Collagen Composition of Healing Medial Collateral Ligament in Rabbits,” *https://home.liebertpub.com/ten*, vol. 12, no. 1, pp. 159–166, Feb. 2006.

[65] C. Erisken, A. Tsiantis, T. D. Papathanasiou, and E. G. Karvelas, “Collagen fibril diameter distribution affects permeability of ligament tissue: A computational study on healthy and injured tissues,” *Comput. Methods Programs Biomed.*, vol. 196, p. 105554, Nov. 2020.

[66] P. S. Mahajan, P. Chandra, V. C. Negi, A. P. Jayaram, and S. A. Hussein, “Smaller anterior cruciate ligament diameter is a predictor of subjects prone to ligament injuries: An ultrasound study,” *Biomed Res. Int.*, vol. 2015, Jan. 2015.

[67] B. L. Proffen, M. Mcelfresh, B. C. Fleming, and M. M. Murray, “A comparative anatomical study of the human knee and six animal species,” 2012.

[68] J. B. Lee *et al.*, “Modification of PLGA Nanofibrous Mats by Electron Beam Irradiation for Soft Tissue Regeneration,” *J. Nanomater.*, vol. 2015, pp. 1–10, 2015.

[69] V. Ottani, M. Raspanti, and A. Ruggeri, “Collagen structure and functional implications,” *Micron*, vol. 32, no. 3, pp. 251–260, Apr. 2001.

[70] K. L. Moffat, A. S. P. Kwei, J. P. Spalazzi, S. B. Doty, W. N. Levine, and H. H. Lu, “Novel Nanofiber-Based Scaffold for Rotator Cuff Repair and Augmentation,” *https://home.liebertpub.com/tea*, vol. 15, no. 1, pp. 115–126, Sep. 2008.

[71] H. Jahani, S. Kaviani, M. Hassanpour-Ezatti, M. Soleimani, Z. Kaviani, and Z. Zonoubi, “The Effect of Aligned and Random Electrospun Fibrous Scaffolds on Rat Mesenchymal Stem Cell Proliferation,” *Cell J.*, vol. 14, no. 1, p. 31, Mar. 2012.

[72] B. Yu and W. E. Garrett, “Mechanisms of non-contact ACL injuries,” *Br. J. Sports Med.*, vol. 41, no. suppl 1, pp. i47–i51, Aug. 2007.